Optically pumped stimulated emission in HgCdTe-based quantum wells: Toward continuous wave lasing in very long-wavelength infrared range

V. Rumyantsev, K. Mazhukina, V. Utochkin, K. Kudryavtsev, A. Dubinov, V. Ya. Aleshkin, A. Razova, D. Kuritsin, M. Fadeev, A. Antonov, et al.

Optically pumped stimulated emission in HgCdTe-based quantum wells: Toward continuous wave lasing in very long-wavelength infrared range

V.V. Rumyantsev[1,2,1)], K.A. Mazhukina[1,2], V.V. Utochkin[1], A.A. Dubinov[1,2], V.Ya. Aleshkin[1,2], M.A. Fadeev[1], D.I. Kuritsin[1], K.E. Kudryavtsev[1], A.A.Razova[1], A.V. Antonov[1], N.N. Mikhailov[3,4], S.A. Dvoretsky[3,5], V.I.Gavrilenko[1,2], F. Teppe[6] and S.V.Morozov[1,2]

[1] Institute for Physics of Microstructures of RAS, Nizhny Novgorod, Russia, 603950

[2] Lobachevsky University of Nizhny Novgorod, Nizhny Novgorod, Russia, 603950

[3] Institute of Semiconductor Physics, Siberian Branch of Russian Academy of Sciences, Novosibirsk, Russia, 630090

[4] Novosibirsk State University, Novosibirsk, Russia, 630090

[5] Tomsk State University, Tomsk, Russia, 634050

[6] Laboratoire Charles Coulomb, UMR 5221, CNRS - University of Montpellier, 34095 Montpellier, France

Amplified interband emission within the 14 – 24 μm range is investigated in HgCdTe-based quantum wells under optical pumping. Carrier lifetimes are shown to be only slightly limited by Shockley-Read-Hall recombination, taking full advantage of the relativistic energy spectra of 2D Dirac fermions in HgCdTe quantum wells in terms of suppressing Auger processes. By carefully optimizing the waveguides and mitigating carrier heating, we achieve amplification thresholds as low as 1.5 - 2 W/cm^2 for a pulse duration of 20 to 500 μs. We estimate that continuous-wave HgCdTe lasers can operate in the Terahertz frequency range if optically pumped by last generation quantum cascade lasers.

[1)] rumyantsev@ipmras.ru

Introduction

For more than 50 years, enormous efforts have been devoted to perfecting techniques of growing the ternary alloy HgCdTe [1], due to its leading role in infrared detection technologies[2]. Molecular beam epitaxy (MBE) of HgCdTe was mastered until the epilayer non-uniformity was less than 0.1% of Cd[3] and the Urbach tail was controlled by the electron-phonon interaction rather than structural disorder[4]. HgCdTe-based quantum wells (QWs) and superlattices were scrutinized both in regard to fundamental effects[5] and potential applications[6]. Currently, multi-QW structures for long-wavelength detectors and emitters can be grown reproducibly with layers composition and thickness controlled via in situ ellipsometry[7].

The quasi-relativistic electron-hole dispersion in HgCdTe QWs hinders the Auger recombination, making it possible to obtain interband gain in the long-wavelength domain up to 31 μm[8]. The wavelength of coherent emission having been pushed beyond the available spectral range of quantum cascade lasers (QCLs), HgCdTe emitters may become of high interest as a part of *Reststrahlen* optics toolkit[9]. Admittedly, the possible applications of interband HgCdTe lasers are quite limited compared to QCLs, but they still can be suitable to a few niche where the particular wavelength and wavelength agile operation are of paramount importance. The quality of QWs and low residual doping could allow HgCdTe emitters to outperform the lead salts lasers[10], which are covering the "QCL gap" between 28 and 50 um at current.

The main obstacle for HgCdTe technology is *p*-*n* junction fabrication in structures with QWs. Unfortunately, the controllable anneal-free *p*-type doping in HgCdTe is a challenging issue, which is difficult to resolve in the short term[1]. However, the undoubted advantages of electrical pumping can be compromised in the long-wavelength lasers, because the carrier injection from "high" barriers can result in a considerable heating of the distribution function in the QWs active region. The carrier heating is indeed detrimental for amplification, as shown in Refs [8,11] in particular. Lowering the barrier height also hinders the emitter's performance by reducing the energetic threshold of Auger recombination[12]. The abovementioned issues suggest that the most straightforward way to realize the potential of HgCdTe QWs is a "frequency converter" operating under optical pumping. The long-wavelength pumping is available mainly from QCLs, which typically have an output of ~1 W at 8 - 12 um (in a continuous wave (CW) regime)[13] decreasing to several tens of mW at longer wavelengths[14]. To be able to exploit such devices for pumping one needs to lower the amplification threshold well below 1 kW/cm^2. In this work, we attempt to realize "heatless" excitation of HgCdTe QWs and plumb the limits of what can be achieved under optical pumping in waveguide heterostructures with HgCdTe QWs as active medium. The results show that lasing should be possible under optical excitation below 10 W/cm^2, allowing quasi-CW operation.

Experimental

Structures under study were MBE-grown on GaAs substrates with in situ control of layer composition and thickness by means of ellipsometry[7]. Thin layer of ZnTe was deposited before the growth of CdTe buffer. The latter was followed by the dielectric waveguide layers containing an array of QWs. The waveguide and QWs were constructed to achieve the best performance. As it is well known, the stimulated emission (SE) occurs when interband gain G is high enough so that

$$(G - \alpha_a)\Gamma = \alpha_p + \alpha_m \qquad (1),$$

where Γ is the optical confinement factor, α_a, α_p, and α_m are the absorption coefficients in the QWs, passive layers and losses for radiation output, respectively. In macroscopic samples the losses α_m can be neglected. Other losses occur mainly from absorption due to free carriers, residual impurities and defects, and lattice vibrations. All three tend to increase with wavelength, especially lattice absorption has a step-like increase when the quanta energy reaches doubled TO phonon energy. This fundamental factor limits QCLs performance based on GaAs and InP, allowing generation only in the minima of two-phonon absorption bands[15]. In contrast to A3B5 materials, the HgCdTe dielectric function is free from two-phonon resonances below 30 um.

Nevertheless, in structures under study it is still important to prevent light from leaking into the GaAs substrate. When the mode penetrates the GaAs substrate, not only it is absorbed by GaAs lattice, but also the electric field in the vicinity of QW array decreases, entailing a drop in the Γ-factor. As a result, larger gain is needed to fulfil the condition of generation. Though the Auger recombination is suppressed in thin HgCdTe QWs, deviations from the ideal relativistic dispersion in the valence band set a finite energetic threshold for the Auger processes[12]. This threshold is the minimal net kinetic energy of carriers for Auger recombination to be allowed by the energy-momentum conservation laws. CCHC process, involving two electrons and a hole, has the lowest threshold energy in thin QWs. As the losses in the passive layers grow, it becomes crucial to keep the optical confinement factor Γ high so that the carrier density required to overcome the losses would not reach the onset of Auger processes. The MBE growth sets some additional limitations. Firstly, the overall thickness of the structure can hardly exceed 20 – 25 um. Secondly, reducing QW thickness, which facilitates higher Auger recombination thresholds, entails increase in inhomogeneity, as indicated by Urbach tail studies and PL linewidth. Therefore, in this work, we used wide enough QWs with a low fraction of cadmium in attempt to balance the suppression of Auger recombination and the impact of inhomogeneity.

Two types of structure designs were implemented to further maximize Γ-factor. In the first one, CdTe buffer was augmented to 15 um to counteract mode leaking into the substrate. In the second one, the “default” CdTe buffer and thinner waveguide layers were grown on heavily doped n++ substrate. Fig. 1 shows the calculated losses for both designs, as well as losses for structures grown on semiinsulating GaAs substrate with “default” thickness of the CdTe buffer (10 um) to illustrate the improvement in Γ-factor. Table I gives details on the parameters of structures studied in this work.

Table 1. The parameters of structures under study. The structure name denotes the GaAs substrate doping (i – semiinsulating, n – doped), the CdTe buffer thickness in microns and the longest emission wavelength at 8 K (after the underscore symbol). Structures with no waveguide and a single QW are denoted as Sqw followed with QW width in Angstrom and cutoff wavelength at 8 K after the underscore symbol. These structures were all grown on a semiinsulating GaAs structures with 5 um CdTe buffer. D_1 – thickness of the first waveguide layer (grown on CdTe buffer from the substrate side), D – thickness of the active region, D_2 – thickness of the covering waveguide layer, x_{wg} – Cd content in the waveguide, N_{QW} – number of QW in the active region, d_{QW} – QW width, x_{QW} – Cd content in the QW, I_{th} – threshold pumping intensity for the SE onset, E_{th} – the threshold energy of CCHC Auger recombination, E_i – the initial kinetic energy of the hole after optical excitation with CO_2-laser, τ – estimated net lifetime for waveguide structures and extracted from PC kinetics for single-QW structures, τ_{RR} – calculated radiative lifetime

Sample	**D_1, μm**	**D, μm**	**D_2, μm**	**x_{wg}**	**N_{QW}**	**d_{QW}, nm**	**x_{QW}**	**I_p, W/cm^2**	**E_{th}**	**E_i**	**τ**	**τ_{RR}**
i10_14	1.9	0.3	3	0.69	5	7.4	0.098	1.5 ± 1	15.9	11.0	40 ± 20	40
i10_22	3.5	0.5	5	0.69	11	6.8	0.067	12 ± 1	21.9	18.6	5	45
i10_25	3.5	0.5	5.1	0.66	15	7.4	0.062	-	20.7	20.6	-	-
i15_24	4.0	0.6	5.0	0.65	15	7.8	0.077	2 ± 1	18.1	19.7	30	35
i15_27	4.0	0.6	5.0	0.65	15	7.8	0.074	-	18.5	19.2	-	-

i10_32	2.7	0.65	3.5	0.65	20	7.6	0.064	-	20.4	20.8	-	-
n10_21	2.6	0.6	3.8	0.62	20	5.2	0.028	8 ± 1	31.0	20.3	8	70
Sqw49_26	-	-	-	0.76	1	4.9	0.001	-	34.4	25.5	10 - 40	100
Sqw48_24				0.7	1	4.8	0.006	-	34.3	24.2	< 5	95
Sqw90_25				0.7	1	9.0	0.087	-	14.3	15.8	10 - 120	80

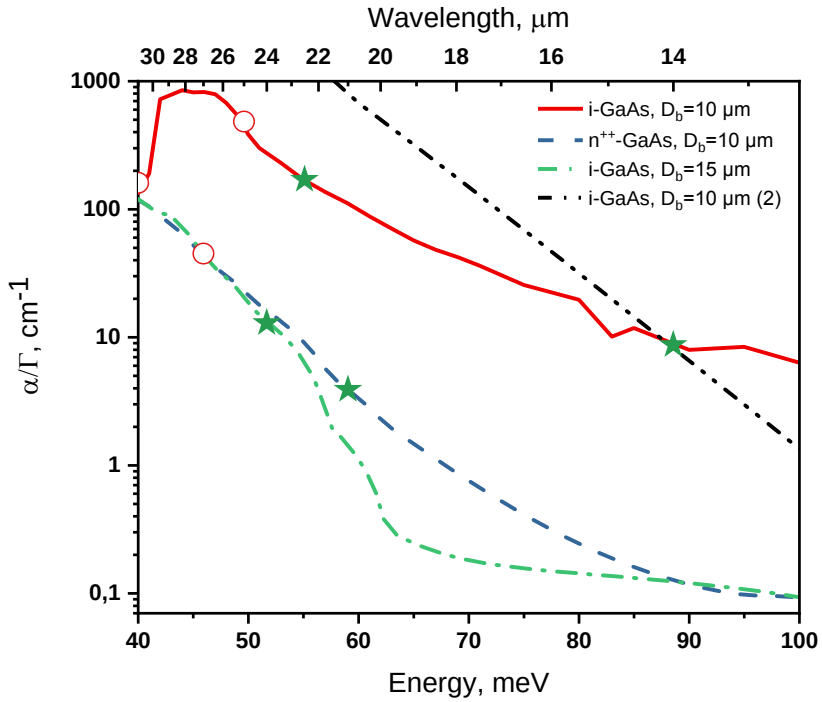

Fig. 1. Mode losses normalized by Γ-factor for different waveguide designs. Symbols represent the waveguide design and emission wavelength for structures under study (stars for structures that provide SE, circles for structures providing only PL)

The samples 5x5 mm^2 were mounted on a cold finger of a closed-cycle cryostat with an available temperature range from 8 to 300 K. The input ZnSe window was used for pumping and the emitted radiation was collected through KRS-5 window. The optical excitation was provided by:
(1) a continuous wave CO_2-laser (operating wavelength 10.6 um) used in optional pulsed regime down to 20 microseconds pulse duration;
(2) continuous wave lasers with operating wavelengths 808 nm/900 nm for excitation into the barriers during PL measurements.
The radiation was collected from the edge of the sample, since the direction perpendicular to the axis of growth of the structure is optimal for amplification. The PL measurements used a configuration in which the excitation was carried out at an angle of 45° to the axis of growth of the structure, and the radiation was collected from the sample surface. To study the SE spectra, the radiation from the samples was guided into the Bruker Vertex 80v Fourier transform infrared (FTIR) spectrometer using a special insert hermetically connecting the closed-cycle cryostat and the spectrometer. This way the narrow lines of atmospheric absorption were eliminated. The FTIR spectrometer operated in the step scan mode. When studying the PL spectra, the radiation from the samples was collected using an elliptical mirror. The scattered radiation of the exciting laser was cut off by the optical filters located on the input window of the spectrometer. Polymethylpentene (TPX) plate was used as a filter when the CO_2-laser was exploited for pumping. HgCdTe detector with a 24 um cutoff or a silicon bolometer were used as detectors.

In addition to waveguide structures, single-QW structures with similar bandgap were used to measure the carrier lifetimes via photoconductivity decay. In this case, the samples were excited with difference frequency generator at operating wavelength of 11 um or 17 um. The acquisition setup included wideband (DC to 200 MHz) amplifier and the oscilloscope with high-frequency limit of 1 GHz so that the time resolution (~ 5 ns) was limited only by the duration of excitation pulse.

Results and discussion

Fig. 2 presents the emission spectra of studied samples for different wavelengths of excitation. In theory, the photoluminescence (PL) spectrum of a QW should follow a step-like 2D density of states near the edge of the interband transitions. Therefore, the low-energy slope of the PL line reflects the inhomogeneous broadening of the sample by having a finite steepness of $W > 2$ meV (consider structure #i10_14, for example). At lattice temperature of 9 K, kT energy of 0.8 meV is considerably lower, and the minimal full width at half maximum (FWHM) of the PL line one could expect is $2W = 4$ meV. Instead, the FWHM of the emission line at 10.6 pumping is much less: a line with the FWHM as low as 0.75 meV is observed in structure #i10_14. Dramatic narrowing of the emission line suggests that SE process is taking place, which is further supported by structure #i15_24. In this case, the low-energy slope is much wider, yet the FWHM of the emission line at 10.6-um-pumping conserves at 0.5 meV from 8 K to 19 K, suddenly broadening at 20 K and then disappearing completely at higher temperatures.

In the simplest model, the PL line is a product of constant density of states and exponential decay from thermal Fermi-Dirac distribution of carriers. For zero inhomogeneous broadening, the spectral line of the spontaneous interband emission in a QW with parabolic bands would have a FWHM of $0.7kT$. At 19 K the FWHM is below $0.7kT = 1.2$ meV testifying that the emission cannot be spontaneous. Note that at 20K the effective temperature of carrier distribution extracted from the high-energy slope of the spectrum is still lower than the lattice temperature suggesting a transient from the SE to the spontaneous radiative transitions is taking place. Aside from narrowing of the emission line, all samples demonstrated a superlinear increase with pumping intensity. Fig 3a shows the dynamics of SE line during the pumping pulse. The rise of the emission line at 24 um with time t is much sharper than the intensity of CO_2-laser grows, which is especially clear at $t > 40$ us. Fig. 3b demonstrates the same effect for integral emission power P_{em} vs. pumping intensity I_p. However, note that such a super-linear dependence on its own can be somewhat misleading because it can also result from the Shockley – Read – Hall (SRH) mechanism saturation. The SRH lifetime may increase considerably with pumping intensity due to saturation of the recombination centers, while the radiative recombination speeds up with carrier density. As a result, the quantum efficiency of the output can grow even in the absence of amplification. Fig. 3b illustrates this point by showing how P_{em} changes with I_p for bulk HgCdTe material, in which no amplification is present. As discussed below, in QWs under study the SRH recombination is noticeable in net carrier lifetime. Therefore, the SE thresholds observed from P_{em} vs. I_p curve were rechecked by spectra measurement in the vicinity of the corresponding pumping intensity. The thresholds, extracted with this approach, are given in Table 1.

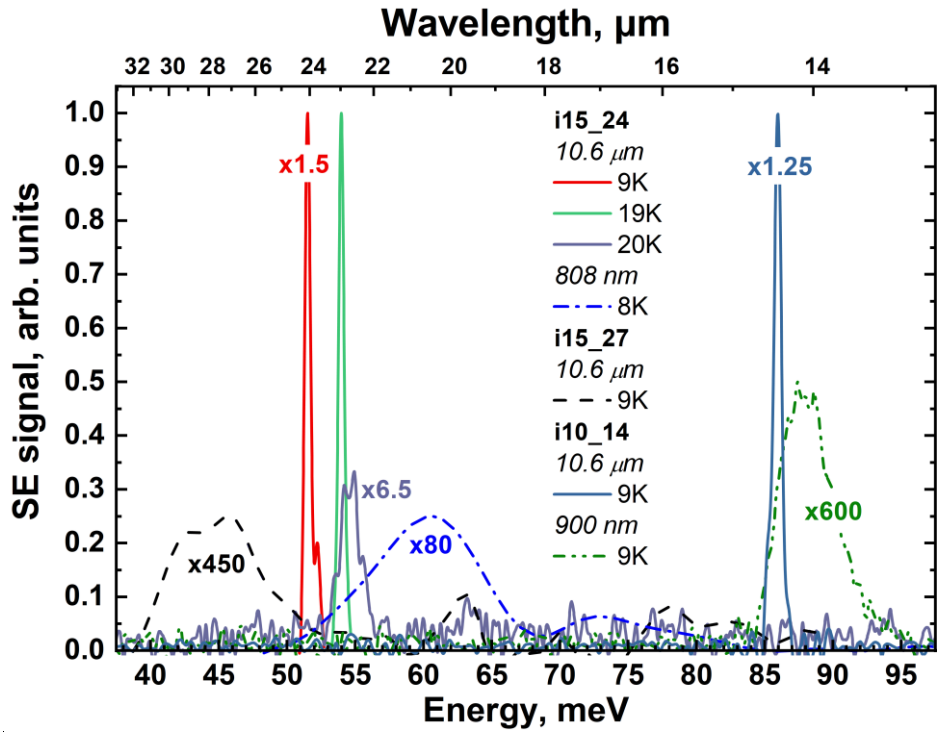

Fig. 2 The emission spectra for structures under study. Multiplication factors demonstrate the relative intensity of PL compared to SE.

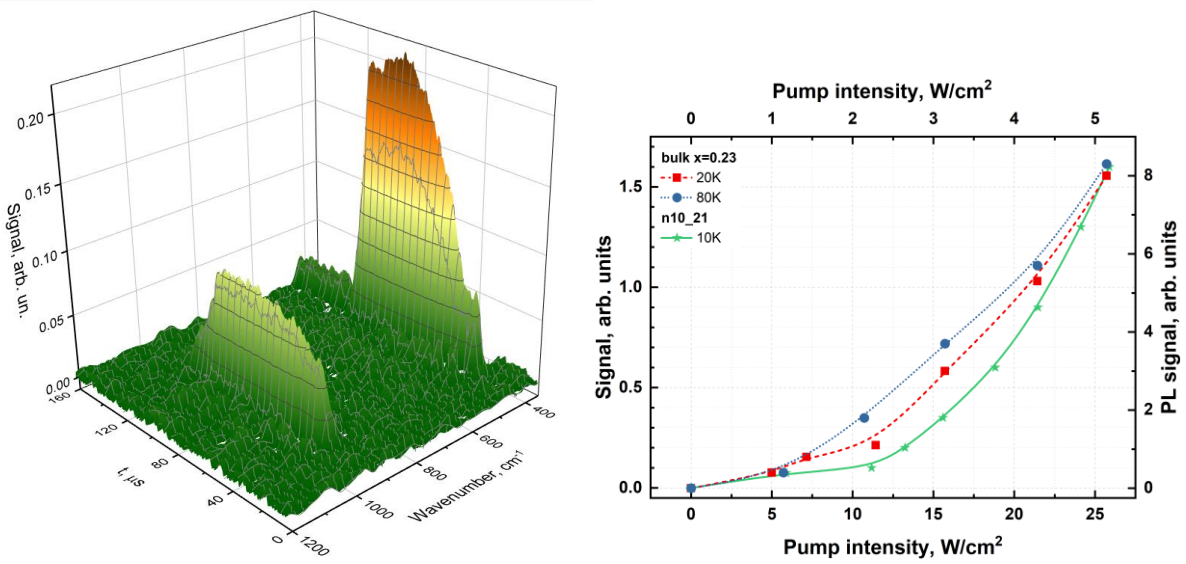

Fig. 3 (a) Time evolution of the emission spectra of structure #i15_24 accompanied by the excitation pulse of pumping CO_2-laser; (b) integral emission power P_{em} vs. pumping intensity I_p for structure #n10_21 and bulk HgCdTe for comparison

The carrier lifetime τ can be estimated from a typical threshold value I_{th} using a simple expression:

$$\tau = \frac{h\nu \cdot n_{th}}{\alpha_{QW} I_{th}} \qquad (2).$$

Here $h\nu = 116$ meV is quanta energy for pumping radiation, $\alpha_{QW} \approx 0.005$ is absorption coefficient for pumping photons is the QW and n_{th} is the threshold carrier density, at which the onset of the amplification happens. Fig. 4 gives the calculated material gain for the structures under study to extract n_{th} at different carrier temperatures. Strictly speaking, the carrier temperature is not known, while the n_{th} is temperature dependent. However, from the fact that SE quenches completely above 20 K in structure #i15_24 we can assume that carrier temperature is below 20 K and consider the carrier threshold density n_{th} to be ~ $10^{10} \pm 5\times10^{9}$ cm^{-2}. Depending on the threshold I_{th}, the carrier lifetime falls into 5 – 40 ns range (see Table 1). Such lifetimes correspond well to the direct measurements of carrier kinetics, performed via PC decay in single QWs with a similar bandgap (Fig. 5).

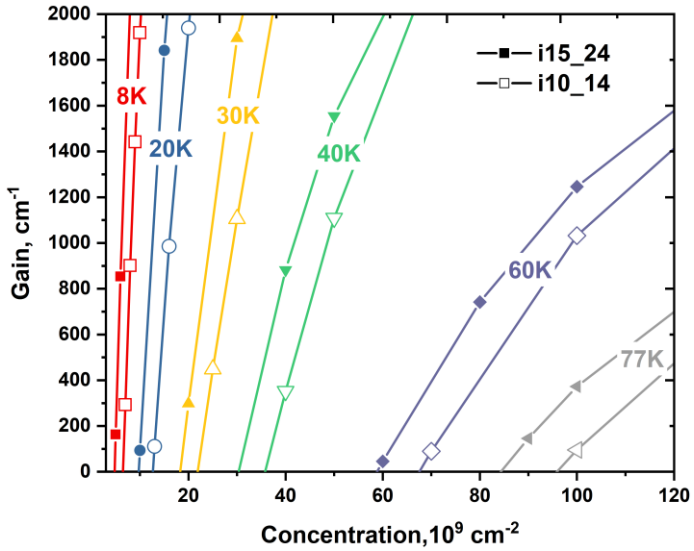

Fig. 4 The material gain for two structures under study calculated for different carrier temperatures

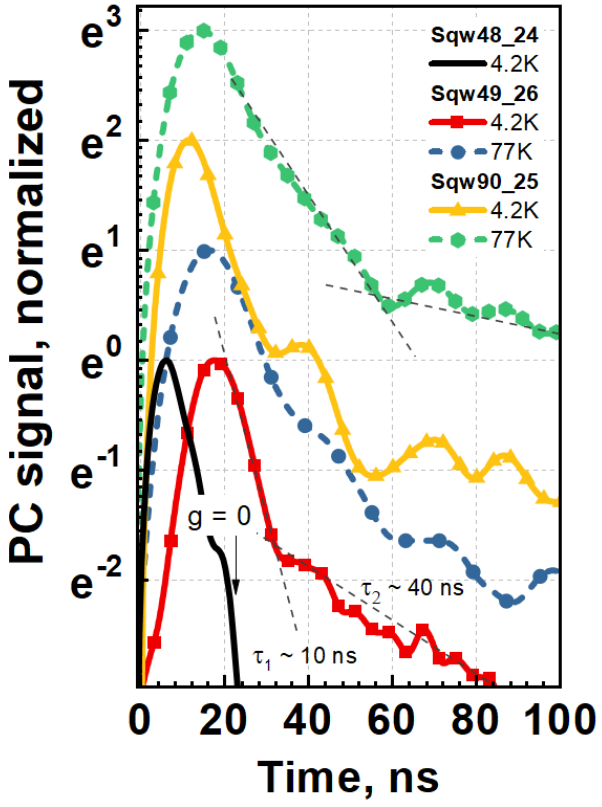

Fig. 5. The PC kinetics for QWs with a bandgap of ~50 meV (cutoff wavelength ~ 25 um) at T = 4.2 K.

For some structures the estimated net lifetime is below the calculated radiative lifetime (see Table 1), suggesting there is a non-radiative contribution of the same order of magnitude. At threshold carrier densities and effective temperatures under consideration, the Auger recombination is completely suppressed[16]. At the same time, the carrier density may not be high enough to saturate SRH recombination. Indeed, the residual defect density is on the order of several units of 10^{14} cm^{-3} in bulk material, grown with the same MBE. Therefore, up to 10^{9} cm^{-2} recombination centers can neighbor the QW within the vicinity of about 30 nm (with proviso of the uniform distribution of recombination centers). This estimate is close to the residual carrier density in best-quality QWs with relatively wide bandgap ~ 120 meV. Note that there is a pronounced deviation from the carrier dynamics predicted for solely radiative recombination[17] when the excess carrier density is comparable to 10^{9} cm^{-2}. In some cases, the residual carrier density is up to several units 10^{10} cm^{-2} and the clear experimental evidence for SRH saturation appear only when carrier concentration is much higher. In Fig. 5, the carrier dynamics is clearly non-exponential even after the excitation pulse *g(t)* has elapsed, revealing a complicated dependence $\tau(n)$. For some PC decay curves a biexponential relaxation is evident, typical for SRH.

The good agreement between the lifetime values, obtained by different methods, support the idea that heating of the carrier distribution is moderate in those samples that provide SE. Returning to Fig. 4, one can notice how abruptly interband gain grows with the carrier density for low temperatures. In particular, the amplification coefficient rises up to 500 cm^{-1} within about a 10% increase in carrier density relative to the onset of gain. Thus, variation of waveguide losses for different designs should have a minor impact on the threshold of SE. The different impact of SRH process on the carrier lifetime can potentially explain the variation of the thresholds observed for different structures and the absence of SE at wavelengths longer than 24 um.

On the one hand, structures #n10_21 and #i10_22 demonstrate similar threshold despite that waveguide losses of structure #i10_22 are 40 times higher. On the other hand, a considerably lower threshold is found in structure #i15_24 with the longest operating wavelength. This may indicate that narrower QWs are prone to higher density of SRH centers. The residual defect density is hard to control and the carrier lifetime can be in sub-ns range leading to thresholds outside the range of the exploited CO2 laser. Fig. 5 shows this case for structure #Sqw48_24, for which the PC response follows the shape of the excitation pulse and thus the carrier lifetime is sure to be less than the time resolution of exploited measurement method ~5 ns. However, since the structures were deposited in a routine growth process it is unnatural to anticipate a strong altering in the density of recombination centers. The remarkable fact is that for all structures that do not demonstrate SE at cw excitation the initial kinetic energy of holes E_{hi} acquired due to optical pumping with 10.6 um is higher than E_{th} (see Table 1). Therefore, a "hot" AR is possible in these structures, taking place right after the excitation. Carrier heating is inevitable during the Auger process. When $E_{hi} < E_{th}$, holes are prevented from AR from during the entire thermalisation process because they occupy only the states with quasi-relativistic E(k) dependence. When $E_{hi} > E_{th}$ the carrier thermalization can be counteracted by the Auger processes happening right after the excitation pulse. Though carrier losses can be tolerable due to such "hot" AR, injecting the additional energy into the electron-hole system can lead to self-sustaining AR and augmented carrier temperature. Consider structure #i15_27, which is identical

to i15_24 in terms of waveguide design. Similar excitation condition in sample #i15_27 result is much broader spectrum at 8 K than that of SE line for structure #i15_24. For #i15_27 the high-energy slope of the PL line corresponds to a carrier temperature of 30 K. Therefore, the absence of SE in #i15_27 is consistent with the fact that the quenching temperature of SE in #i15_24 is 20 K. This heating introduced by AR can be avoided either in structures with larger E_{th} or by using pumping with longer wavelength.

To summarize, obviating carrier heating and Auger recombination allows low carrier temperature at which amplification coefficient can be huge, promising that a wide wavelength range can be covered. Although apparently thresholds are controlled by SRH recombination, in the best structures this process has a marginal importance and the estimated carrier lifetimes approach those of pure radiative recombination. As shown in Fig.5 carrier lifetimes do not significantly degrade when the temperature reaches 77 K. Therefore, the threshold increase can be expected to take place according to $n_{th}(T)$ from Fig. 4, which gives an estimation of $I_{th}(T = 77\ K) \sim 10 I_{th}(T = 8\ K)$. It should be noted that in this work the pump radiation was only exploited to the extent of about 10% due to the below-barrier excitation, however more efficient pumping is therefore possible.

Microcavities with reasonable Q-factor can be formed by either wet or ion etching from HgCdTe structures, as demonstrated in Refs.. Considering a microdisc of ~ 200 um diameter and the corresponding pump beam spot, one obtains several mW for the threshold output power. Such values are achievable with CW QCLs, even at room temperature, and not only in the vicinity of 10 μm but even up to 16 μm. Thus, the excess energy injected by photons pumping can be further reduced compared to this work and it is possible to prepare the initial carrier distribution for which even "hot" Auger recombination is strongly suppressed. This approach opens the way to the creation of compact optical converters based on HgCdTe heterostructures operating in the "Reststrahlen" gap of III-V semiconductor-based QCLs.

References

[1] Wen Lei, Jarek Antoszewski, and Lorenzo Faraone, Applied Physics Reviews **2** (4), 041303 (2015).

[2] A. Rogalski, Reports on Progress in Physics **68** (10), 2267 (2005).

[3] Jun Shao, Lu Chen, Wei Lu, Xiang Lü, Liangqing Zhu, Shaoling Guo, Li He, and Junhao Chu, Applied Physics Letters **96** (12), 121915 (2010); Vasily S. Varavin, V. V. Vasiliev, Sergey A. Dvoretsky, Nikolay N. Mikhailov, Victor N. Ovsyuk, Yuri G. Sidorov, A. O. Suslyakov, M. V. Yakushev, and Alexander L. Aseev, Proceedings of SPIE **5136**, 381 (2003).

[4] Vladimir Rumyantsev, Anna Razova, Mikhail Fadeev, Vladimir Utochkin, Nikolai Mikhailov, Sergey Dvoretsky, Vladimir Gavrilenko, and Sergey Morozov, Optical Engineering **60** (8), 082007 (2020).

[5] Lukas Lunczer, Philipp Leubner, Martin Endres, Valentin L. Müller, Christoph Brüne, Hartmut Buhmann, and Laurens W. Molenkamp, Physical Review Letters **123** (4), 047701 (2019); S. Gebert, C. Consejo, S. S. Krishtopenko, S. Ruffenach, M. Szola, J. Torres, C. Bray, B. Jouault, M. Orlita, X. Baudry, P. Ballet, S. V. Morozov, V. I. Gavrilenko, N. N. Mikhailov, S. A. Dvoretskii, and F. Teppe, Nature Photonics **17** (3), 244 (2023).

[6] S. Ruffenach, A. Kadykov, V. V. Rumyantsev, J. Torres, D. Coquillat, D. But, S. S. Krishtopenko, C. Consejo, W. Knap, S. Winnerl, M. Helm, M. A. Fadeev, N. N. Mikhailov, S. A. Dvoretskii, V. I. Gavrilenko, S. V. Morozov, and F. Teppe, APL Materials **5** (3), 035503 (2017).

[7] V. A. Shvets, N. N. Mikhailov, D. G. Ikusov, I. N. Uzhakov, and S. A. Dvoretskii, Optics and Spectroscopy **127** (2), 340 (2019).

[8] V. V. Rumyantsev, A. A. Dubinov, V. V. Utochkin, M. A. Fadeev, V. Ya. Aleshkin, A. A. Razova, N. N. Mikhailov, S. A. Dvoretsky, V. I. Gavrilenko, and S. V. Morozov, Applied Physics Letters **121** (18), 182103 (2022).

[9] K. Feng, W. Streyer, Y. Zhong, A. J. Hoffman, and D. Wasserman, Opt. Express **23** (24), A1418 (2015); M. Lamperti, R. Gotti, D. Gatti, M. K. Shakfa, E. Cané, F. Tamassia, P. Schunemann, P. Laporta, A. Farooq, and M. Marangoni, Communications Physics **3** (1), 1 (2020).

[10] A. R. Adams, C. T. Elliott, A. Krier, B. N. Murdin, and M. Tacke, Philosophical Transactions of the Royal Society of London. Series A: Mathematical, Physical and Engineering Sciences **359**, 547 (2001).

[11] V. V. Rumyantsev, M. A. Fadeev, V. Ya Aleshkin, A. A. Dubinov, V. V. Utochkin, A. V. Antonov, D. A. Ryzhov, D. I. Kuritsin, V. I. Gavrilenko, Z. F. Krasilnik, C. Sirtori, F. Teppe, N. N. Mikhailov, S. A. Dvoretsky, and S. V. Morozov, Journal of Infrared, Millimeter, and Terahertz Waves **41** (7), 750 (2020).

[12] V. Y. Aleshkin, A. A. Dubinov, V. V. Rumyantsev, and S. V. Morozov, Journal of physics: Condensed matter **31** (42), 425301 (2019).

[13] B. Schwarz, C. A. Wang, L. Missaggia, T. S. Mansuripur, P. Chevalier, M. K. Connors, D. McNulty, J. Cederberg, G. Strasser, and F. Capasso, ACS photonics **4** (5), 1225 (2017).

[14] Alexei N. Baranov, Michael Bahriz, and Roland Teissier, Opt. Express **24** (16), 18799 (2016).

[15] Keita Ohtani, Mattias Beck, Martin Josef Süess, Jérôme Faist, Aaron Maxwell Andrews, Tobias Zederbauer, Hermann Detz, Werner Schrenk, and Gottfried Strasser, ACS photonics **3** (12), 2280 (2016); K. Ohtani, M. Beck, and J. Faist, Applied Physics Letters **105** (12), 121115 (2014).

[16] V. Ya. Aleshkin, V. V. Rumyantsev, K. E. Kudryavtsev, A. A. Dubinov, V. V. Utochkin, M. A. Fadeev, G. Alymov, N. N. Mikhailov, S. A. Dvoretsky, F. Teppe, V. I. Gavrilenko, and S. V. Morozov, Journal of Applied Physics **129** (13), 133106 (2021).

[17] V. Ya Aleshkin, A. A. Dubinov, V. V. Rumyantsev, M. A. Fadeev, O. L. Domnina, N. N. Mikhailov, S. A. Dvoretsky, F. Teppe, V. I. Gavrilenko, and S. V. Morozov, Journal of Physics: Condensed Matter **30** (49), 495301 (2018).